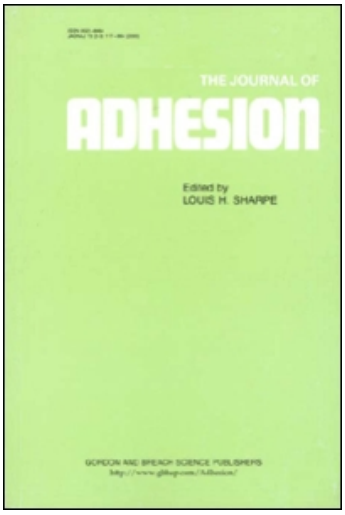

The Journal of Adhesion

Publication details, including instructions for authors and subscription information:
http://www.informaworld.com/smpp/title~content=t713453635

Time Dependent Crack Growth and Loading Rate Effects on Interfacial and Cohesive Fracture of Adhesive Joints

M. D. Rakestraw[a]; M. W. Taylor[a]; D. A. Dillard[a]; T. Chang[b]
[a] Engineering Science and Mechanics Department, Vifginia Polytechnic Institute and State University, Blacksburg, VA, USA [b] Materials Science and Engineering Department, Virginia Polytechnic Institute and State University, Blacksburg, VA, USA

To cite this Article Rakestraw, M. D. , Taylor, M. W. , Dillard, D. A. and Chang, T.(1995) 'Time Dependent Crack Growth and Loading Rate Effects on Interfacial and Cohesive Fracture of Adhesive Joints', The Journal of Adhesion, 55: 1, 123 — 149
To link to this Article: DOI: 10.1080/00218469509342411
URL: http://dx.doi.org/10.1080/00218469509342411

J. Adhesion, 1995, Vol. 55, pp. 123–149
Reprints available directly from the publisher
Photocopying permitted by license only

Time Dependent Crack Growth and Loading Rate Effects on Interfacial and Cohesive Fracture of Adhesive Joints*

M. D. RAKESTRAW, M. W. TAYLOR and D. A. DILLARD**

Engineering Science and Mechanics Department, Virginia Polytechnic Institute and State University, Blacksburg, VA 24061-0219, USA

T. CHANG

Materials Science and Engineering Department, Virginia Polytechnic Institute and State University, Blacksburg, VA 24061-0237, USA

(Received January 27, 1995; in final form July 6, 1995)

Double cantilever beam fracture specimens were used to investigate rate dependent failures of model epoxy/steel adhesively bonded systems. Quasi-static tests exhibited time dependent crack growth and the maximum fracture energies consistently decreased with debond length for constant crosshead rate loading. It was also possible to cause debonding to switch between interfacial and cohesive failure modes by simply altering the loading rate. These rate dependent observations were characterized using the concepts of fracture mechanics. The time rate of change of the strain energy release rate, dG/dt, is introduced to model and predict failure properties of different adhesive systems over a range of testing rates. An emphasis is placed on the interfacial failure process and how rate dependent interfacial properties can lead to cohesive failures in the same adhesive system. Specific applications of the resulting model are presented and found to be in good agreement when compared with the experimental data. Finally, a failure envelope is identified which may be useful in predicting whether failures will be interfacial or cohesive depending on the rate of testing for the model adhesive systems.

KEY WORDS Adhesive failure; cohesive failure; double cantilever beam; interfacial failure; fracture mechanics; loading rate effects; rubber-modified epoxy; time-dependent fracture, subcritical crack growth, stick-slip behavior, viscoelastic debonding.

INTRODUCTION

Adhesive bonding has many potential advantages over conventional fastening techniques, including weight and fabrication cost savings, the ability to join dissimilar materials, and a more efficient stress distribution in the substrates.[1] However, before these advantages can be realized, assurance is needed that a given adhesive system can withstand the service conditions which are expected over the life of a particular

*One of a Collection of papers honoring James P. Wightman, who received the *13th Adhesive and Sealant Council Award* at the ASC's 1993 Fall Convention in St. Louis, Missouri, USA, in October 1993.

**Corresponding author.

structure. Failure processes in the bondline are often time and rate dependent, and thus the ability to predict accurately the long term durability will ultimately require the appropriate analysis of these debonding processes.

Rubber-toughened epoxy adhesives exhibit high modulus, good creep resistance, and moderate resistance to fracture[2,3] but have been shown to be temperature and rate-dependent.[4-11] In addition to investigations on the bulk adhesive itself, a number of studies have also shown that interfacial properties become increasingly important when studying the long-term durability of adhesively bonded structures, since failures tend to move to the interface when subjected to harsh environmental conditions.[12-17] It is evident that any complete durability testing and predictive methodology should be capable of studying and characterizing both interfacial and cohesive rate-dependent failures.

A number of investigators have looked at the analysis of rate-dependent fracture processes, including Schapery[18,19] and Knauss.[20] Knauss and Losi[21] extended the analysis to the case of a viscoelastic material bonded to an elastic substrate. A great deal of experimental research has been reported in the area of time-dependent failure of rubber-based and pressure sensitive adhesives (see for example, Gent and Petrich.[22]) Maugis[23] has extended the physics governing time-dependent contact problems to subcritical crack growth in bonded joints. Although we were not aware of his work at the time we conducted our studies, many of our observations are consistent with his conclusions. A further complicating feature of adhesively bonded joints is that the locus of failure may be cohesive, adhesive, or mixed. If the time-dependent nature of the interphase region and the bulk adhesive are different, altering the rate of testing can cause the failure to change modes. This phenomenon has been widely observed, especially for rubber-based or pressure sensitive adhesives such as reported by Gent and Petrich.[22]

The present authors used fracture mechanics concepts to quantify the static, fatigue, and environmental performance of model epoxy/steel adhesive systems in past studies.[24-28] These materials represent simple model systems which may be relevant to certain automotive adhesive bonds. The present study uses fracture mechanics concepts to characterize the rate-dependent failures which were observed in the double cantilever beam (DCB) specimens used in this research effort. Both rate-dependent interfacial and cohesive failures are modeled in terms of the time rate of change of the strain energy release rate, dG/dt. First, the interfacial failure process is addressed by separating dG/dt into two fundamental components. The first component is the induced (or controlled) loading which is applied to the specimen through mechanical means. The other component is the unloading process which results when cracking/debonding occurs. This represents the natural or inherent time-dependent debonding response of the crack tip to a loading level above the debonding threshold. By combining the induced and natural loading processes, it is possible to examine their combined effect on the mechanical response of the specimens used in the experiments. Predictions of the rate-dependent interfacial model are used and compared with the experimental observations. The model was further extended to include cohesive failures which were frequently observed at higher loading rates. After modeling the rate-dependent transition between interfacial and cohesive failure, this information is used in conjunction with the testing rate, specimen geometry, and the natural inter-

facial failure rate to identify a failure envelope which can be used to predict whether an interfacial or cohesive failure will occur in experiments.

EXPERIMENTAL

Five model epoxy systems with various amounts of rubber-toughener were used as the adhesives for this study. The model epoxy systems were composed of a liquid bisphenol A-type resin, a curing agent, a curing accelerator, a filler, and an epoxy-terminated toughener. The epoxy resin used was D.E.R. 331®†, a low molecular weight, liquid bisphenol A-type resin available from The Dow Chemical Company. The curing agent used was dicyandiamide ("dicy"). A tertiary amine accelerator, 3-phenyl-1,1 dimethyl urea (PDMU) was used to reduce cure times. M-5 silica, which is a slightly acidic, hydrophillic fumed silica produced by the Cabot Corporation, was used as a filler. The toughener used was Kelpoxy G272-100, a concentrate of an epoxy-terminated elastomeric copolymer designed by Reichhold Chemicals as an additive or modifier to toughen epoxies, epoxy novalacs, and PVC plastisols. Epoxy resin blends containing Kelpoxy exhibit elastomer particles of .01–10 micron diameter which impede the propagation of cracks. The epoxide equivalent weight is approximately 340 g/eq. Compositions of the model systems are given in Table I. Additional details about the mixing, curing, and specimen preparation may be found in Refs. 25 and 28.

The test geometry used in this research was the conventional double cantilever beam (DCB) specimen which is shown in Figure 1. Unless otherwise noted, the surfaces of the 6.4 mm thick 1018 steel panels were cleansed with an acetone wipe prior to the bonding process. (Since substrates are not typically surface treated for automotive applications, the acetone wipe was used simply to provide some degree of surface uniformity among specimens.) Panels with dimensions of 360 × 230 mm were cured at a temperature of

TABLE I
Model adhesive formulations (grams).

	Formulation Designation				
Component	A	B	C	D	E
D.E.R. 331	88.5	78.4	69.1	60.9	52.6
DICY	4.4	4.2	4.1	3.9	3.8
PDMU	1.8	1.7	1.6	1.6	1.5
M-5 Silica	5.3	5.1	4.9	4.7	4.5
Kelpoxy G272	0.0	10.6	20.3	28.9	37.6
Totals:	100	100	100	100	100
% Rubber Approximate*	0	4.2	8.1	11.6	15.0

* Since Kelpoxy is an epoxy-terminated copolymer containing approximately 40% rubber.

† D.E.R. is a registered trademark of The Dow Chemical Company.

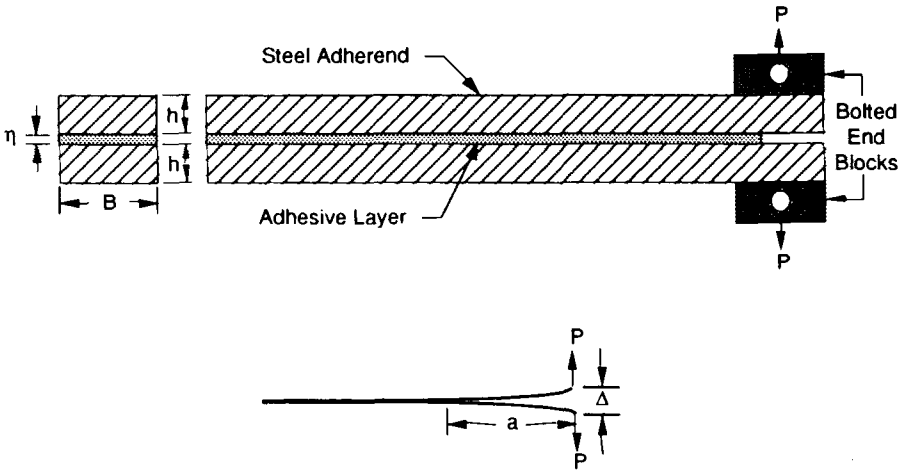

FIGURE 1 The conventional double cantilever beam fracture specimen.

170 °C and a pressure of 33 kPa for a period of 90 minutes. A water jet cutter was used to slice the bonded panels into the final DCB specimens with dimensions of 230 mm × 25.4 mm. The nominal bond thickness used was 0.8 mm.

The quasi-static DCB tests were carried out at ambient conditions ($T \approx 23$ °C) on a screw-driven Instron 4505 testing frame. Data acquisition and test frame control was performed through a GPIB interface using LabVIEW® software. As the specimens were loaded in displacement control, visual observations of crack growth (using a traveling microscope) along with load-deflection and load-time curves were used to detect critical events taking place. Crack length readings were also periodically taken when there was sufficient confidence in those values. Details of specimen fabrication and testing procedures may be found in Ref. 25.

Double Cantilever Beam Data Analysis

The strain energy release rate, G, was determined for the DCB specimens using the compliance method with corrections for crack length offset and adherend stiffness as given in Ref. 29. The beam theory equations used for a uniform width DCB specimen under both load and displacement control are given by:

$$G = \frac{P^2(a+x)^2}{B(EI)_{\text{eff}}} \quad \text{and} \quad G = \frac{9\Delta^2(EI)_{\text{eff}}}{4B(a+x)^4} \tag{1a, b}$$

respectively, where P is the load applied to the specimen, a is crack length (defined as the projected distance from the point of load application to the debond tip), B is the specimen width, $(EI)_{\text{eff}}$ is the effective flexural rigidity of the DCB specimen, x is the crack length offset and Δ is the opening displacement at the point of load application. The parameters $(EI)_{\text{eff}}$ and x are computed from the experimental data according to:

$$(EI)_{\text{eff}} = \left(\frac{2}{3m^3}\right) \quad \text{and} \quad x = \frac{b}{m} \tag{2a, b}$$

where the experimental coefficients m and b are the slope and y-intercept, respectively, of the cube root of the measured compliance, $C^{1/3} = (\Delta/P)^{1/3}$, when plotted as a linear function of crack length, as shown in Figure 2. By recognizing this linear relationship with experimental data, a value for crack length, a, can be estimated for a given Δ and P, and thus one can obtain strain energy release rate values from Eq. 1 without manually reading the crack length. A load-deflection data set with time also makes it possible to calculate rates of crack growth using this method. Correction factors related to adherend shear were not needed because the initial crack lengths were always significantly larger than the adherend thickness, and large deflection corrections[29] were not needed because of the stiffness of the relatively thick adherends used to avoid plastic yielding.

Observations

A typical load-hold-unload cycle observed in this study for interfacial cracking is given in Figure 3. At point 1 the unloaded specimen had an original crack length a_i. Load was then applied at a constant displacement rate (usually 1 mm/min) from point 1 to point 3. From point 1 to point 2 load and deflection increased linearly and the applied strain energy release rate went up parabolically since the crack was not growing. At point 2 the crack "initiates" at a strain energy release rate value of G_c. Initiation was defined to be when the load-time data began to deviate from linearity. Visual confirmation of this

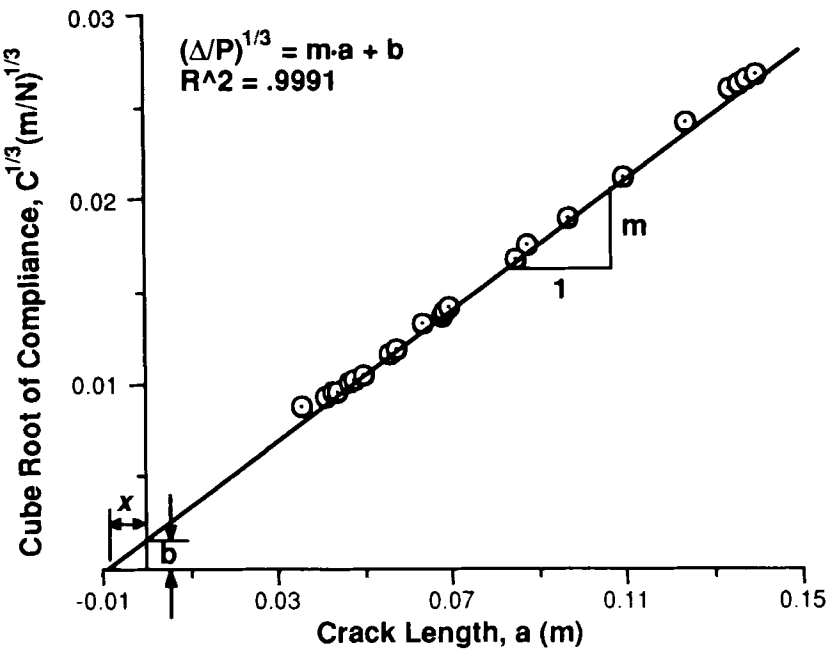

FIGURE 2 Typical experimental compliance-crack length calibration results for a DCB specimen (Adhesive D).

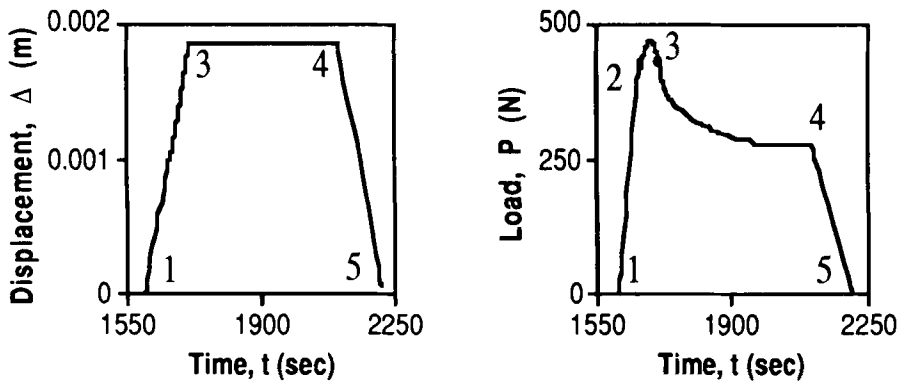

FIGURE 3 The deflection-time (controlled) and load-time (response) curves for a typical loading cycle (Cycle #3 of Fig. 4).

debond initiation has also been made using a microscope. From point 2 to point 3, while crack growth is occurring, G (as well as P) increased, went through a maximum, G_{max}, then decreased. From point 3 to point 4 the displacement was held constant and the crack continued to grow until it arrested at point 4 at a value of G_a. To expedite the testing, the crack was assumed to be arrested when the load dropped less than 1N in 60 seconds. The specimen was then unloaded from point 4 to point 5 to check for permanent set. For the adherend thickness used herein, no permanent set was observed. This loading cycle could be repeated several times for each specimen.

Figure 4 shows results from five load-hold-unload cycles for a typical specimen. For all of the specimens tested, it was observed that the initiation of a crack occurred at approximately the same strain energy release rate as the arrest value of the previous loading cycle. Although these values are relatively constant across the entire length of the specimen, a slight downward trend with crack length can be observed. This effect is believed to be due to the criterion used to determine when the crack had arrested. The values of G_{max}, however, show a very distinct decrease with crack length. This is clear when one compares the peaks of the loading curves with the iso-G_{max} curve based on the average G_{max} for the five loading cycles. Figure 5 shows how the G_c or G_a values and the G_{max} values varied for the different amounts of rubber toughener. Error bars indicate one standard deviation. All of the failures referred to above appeared to be interfacial to the naked eye. XPS analysis of the steel adherend after fracture suggests that the carbon-to-iron ratio is slightly higher than on unbonded steel. Also there appears to be more organic hydroxyl groups, suggesting that the actual failure locus is very close to the steel surface, but that some polymer is being left on the substrate.[24]

Altering the displacement rates for all specimens could sometimes alter the mode of failure from adhesive to cohesive or *vice versa*, with correspondingly large changes in fracture energies. Table III lists the strain energy release rates for both adhesive and cohesive failures. In general, increasing the displacement rate could cause specimens which predominately fail interfacially to fracture cohesively. Equivalently lowering the displacement rate could cause cohesive cracks to switch to the interface. In a previous

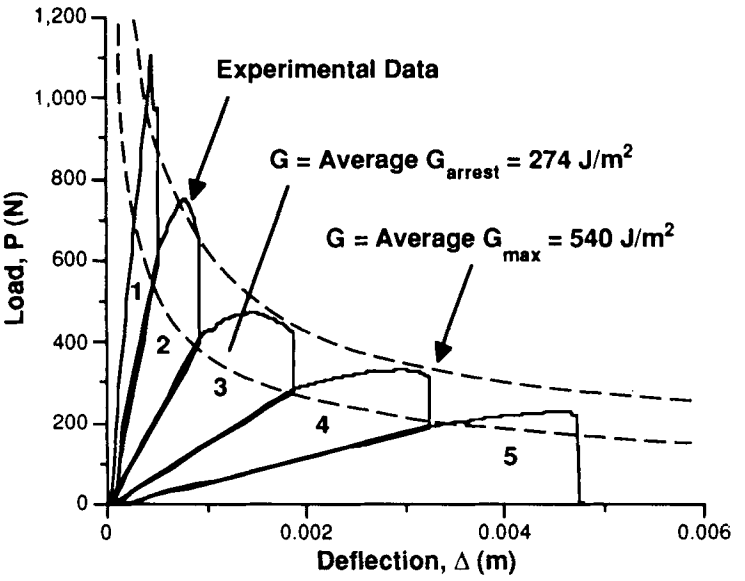

FIGURE 4 Typical load-deflection curve from a quasi-static DCB test showing five load-hold-unload cycles and Iso-*G* curves (Adhesive D).

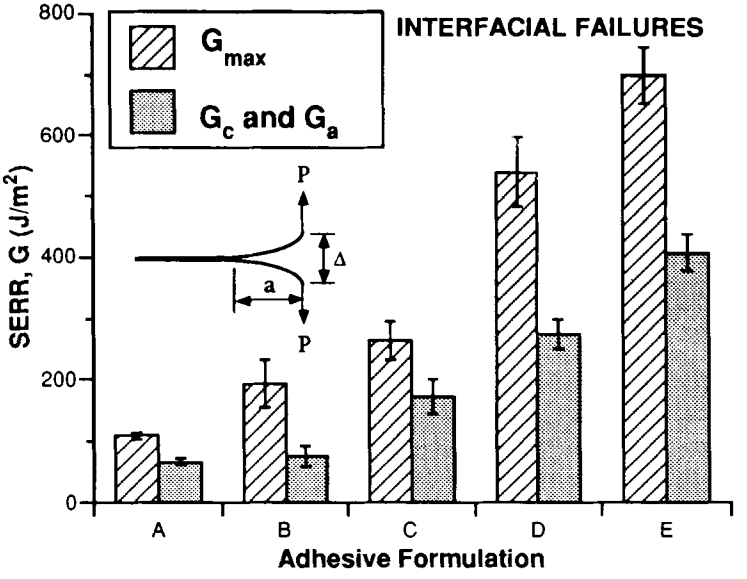

FIGURE 5 Maximum and arrest values of the strain energy release rate (SERR) for model adhesive formulations (1 mm/min testing speed).

TABLE II
Fracture data used in the predictive model

Adhesive D	
Sample	11-30#1b
Specimen Width, B (m)	0.0259
x(m)	0.0089
$(EI)_{eff}$(N·m^2)	115.4
a_0(m)	0.032
$G_c \approx G_a$(J/m^2)	274
z(Cycle#1)	7.55
A (Cycle#1)	2.80E-20

TABLE III
Measured strain energy release rates for cohesive and interfacial failures in DCB specimens (J/m^2). (The error is one standard deviation)

	Interfacial Ga	G_{max}	Cohesive
A	68 ± 8	110 ± 9	287 ± 72
B	78 ± 24	196 ± 47	639 ± 103
C	172 ± 41	266 ± 46	1141 ± 90
D	274 ± 42	540 ± 76	1086 ± 46
E	376 ± 81	699 ± 68	1867 ± 206

study[24] it was shown that slight variations in surface pretreatment, adhesive chemistry or cure conditions could also cause failures to become cohesive in nature. Observations of the interfacial and cohesive failures may be summarized as follows:

Summary of Interfacial Failure Observations

(1) Crack growth began at a loading level of G_c, went through a maximum G_{max}, and started to decrease during constant displacement rate testing.
(2) As crack lengths increased, G_{max} values consistently decreased when a constant displacement rate was maintained for each loading cycle.
(3) Holding the displacement constant above G_c caused debonding to continue but arrest with time at a level of G_a.
(4) Debonding initiated and arrested at about the same load level (*i.e.* $G_c \approx G_a$).
(5) During debonding, if displacement was not stopped after reaching G_{max} the strain energy release rate would decrease and approach G_a under constant crosshead rate loading.
(6) Load-deflection curves contained "gaps" if the hold portion of the testing procedure was omitted and the specimen was immediately unloaded after reaching G_{max}, suggesting continued debonding during the deboding cycle while G remained higher than G_a.
(7) Cohesive failures could be induced by increasing the displacement rate, but required a much higher amount of energy for propagation.

(8) The fracture energies of these interfacial failures were much lower than the fracture energies of the bulk adhesive as determined from single edge notched bend (SENB) specimens, ASTM D-5045.

Summary of Cohesive Failure Observations

(9) Interfacial failures could be induced by decreasing or stopping the displacement rate. These failures occurred at much lower values of available strain energy release rate.

(10) Unlike the interfacial failures which required higher amounts of energy for rapid debond propagation, the cohesive failures required less energy for propagation at higher rates. This behavior results in the stick-slip patterns common to glassy failure events. At longer debond lengths, higher critical strain energy release rates were measured, presumably because of the rate of loading effect under constant crosshead rate testing.

MODELING RATE-DEPENDENT INTERFACIAL FAILURES

The rate dependence of adhesive debonding is widely recognized, and attempts to minimize the effect in laboratory tests have been given, for example, in ASTM D-3433.[30] Rather than ignoring this effect, this paper will seek to explore the time dependence, and utilize this response in developing models which may be useful in characterizing the time dependence. Both rate-dependent loading and time-dependent crack growth concepts will be used in the subsequent procedures. A distinction, however, is made between global parameters related to the applied load or displacement, and the local parameters which relate to the strain energy release rate or stress intensity factor associated with the debond.

The traditional approach for modeling rate-dependent crack growth has involved the concept of the cracking or debonding rate, da/dt, to define the failure process rate.[9, 10, 14, 15, 21, 23, 31–35] As will be discussed, there are several disadvantages associated with this method, including the inability to compare different loading rates applied to specimens with stationary cracks. In a few instances, rate dependent loading analyses for bulk polymer fracture tests have used the concept of dK/dt, the time rate of change of the stress intensity factor, K, with time.[7] Specifying a global loading rate such as $d\Delta/dt$ or dP/dt directly relates to the time rate of change of the local stress intensity factor for the crack, dK/dt. Since the strain energy release rate is used to characterize the local loading level for a DCB specimen, a possible local rate parameter would be dG/dt, the time rate of change of the applied strain energy release rate.

A Rate-Dependent Interfacial Failure Model

From Eq. 1b, the only quantities which may influence G during a given test are Δ and a. Therefore, when considering the time rate of change of G for displacement control, the total derivative becomes:

$$\frac{dG}{dt} = \left(\frac{\partial G}{\partial \Delta}\right)\frac{d\Delta}{dt} + \left(\frac{\partial G}{\partial a}\right)\frac{da}{dt}. \tag{3}$$

When discussing dG/dt one must be careful since two components exist. One part is actually applied to the specimen by mechanical means (that which is associated with $d\Delta/dt$) and the other is the unloading of the specimen because of crack growth (that which is associated with da/dt). In order to avoid confusion, the following notation is introduced:

$$\dot{G} = (\dot{G})_a + (\dot{G})_\Delta \tag{4}$$

where $\dot{G}$ is the total or net time rate of change in G, $(\dot{G})_a$ is the time rate of change of G due to grip displacement (*i.e.* at fixed crack length), and $(\dot{G})_\Delta$ is the time rate of change of G due to crack growth (*i.e.* at fixed grip displacement). Throughout, the dot is understood to represent the first derivative with respect to time. For our purposes, it is convenient to refer to $(\dot{G})_a$ as the induced loading rate (since it is mechanically induced by the grip displacement), and refer to $(\dot{G})_\Delta$ as the natural unloading rate (since it is the natural rate of decline in G as the debond propagates). For the DCB specimen loaded in displacement control, the following is obtained for each term from Eq. 1b:

$$(\dot{G})_a = \frac{9\Delta(EI)_{\text{eff}}}{2B(a+x)^4}\dot{\Delta} \quad \text{and} \quad (\dot{G})_\Delta = -\frac{9\Delta^2(EI)_{\text{eff}}}{B(a+x)^5}\dot{a} \tag{5a, b}$$

Substituting Eq. 5 into Eq. 4 gives the net loading rate:

$$\dot{G} = \frac{9(EI)_{\text{eff}}}{B(a+x)^4}\left[\frac{\dot{\Delta}}{2\Delta} - \frac{\dot{a}}{a+x}\right] \tag{6}$$

It is convenient to rewrite these equations in terms of the strain energy release rate. This can be done by solving Eq. 1b for Δ and substituting the result into Eq. 5 to give:

$$(\dot{G})_a = \frac{3\dot{\Delta}}{(a+x)^2}\sqrt{\frac{G(EI)_{\text{eff}}}{B}} \quad \text{and} \quad (\dot{G})_\Delta = -\frac{4G\dot{a}}{(a+x)}. \tag{7a, b}$$

Substituting these terms into Eq. 6 gives the net loading rate:

$$\dot{G} = \frac{3\dot{\Delta}}{(a+x)^2}\sqrt{\frac{G(EI)_{\text{eff}}}{B}} - \frac{4G\dot{a}}{(a+x)}. \tag{8}$$

Characterizing the Induced Loading Rate

In this section the influence of the induced loading rate will be addressed by considering a stationary debond ($\dot{a} = 0$). If displacement control is being used, the induced loading rate is given by:

$$(\dot{G})_a = \frac{3}{(a+x)^2}\sqrt{\frac{G(EI)_{\text{eff}}}{B}}\frac{d\Delta}{dt}. \tag{9}$$

Using a similar procedure as above for load control gives:

$$(\dot{G})_a = 2(a + x)\sqrt{\frac{G}{B(EI)_{\text{eff}}}}\frac{dP}{dt} \tag{10}$$

It can be seen from Eq. 9 and 10 that for a given strain energy release rate, G, and for a constant global loading rate (*i.e.* $d\Delta/dt = \text{const}$ or $dP/dt = \text{const}$), the induced loading rate is a function of crack length, a, and is thus not constant over the specimen geometry. Figure 6 depicts this result, showing that the induced loading rate prior to failure can vary by over an order of magnitude when typical displacement controlled test conditions are used. Such behavior has led to DCB testing procedures which recommend increasing the crosshead rate as the debond grows.[30]

Characterizing the Natural Unloading Rate

We now examine the second term in Eq. 4, the **response** of the debond tip to the mechanically applied **input**. A common approach for characterizing the failure rate of many materials is to model the crack growth rate, da/dt, as a function of either the applied stress intensity factor, K, or the applied strain energy release rate, G. Log-log plots of this information are commonly used because a considerable portion of the data can often be modeled using a simple power law relationship of the form:

$$\frac{da}{dt} = c_1 \cdot G^n \tag{11}$$

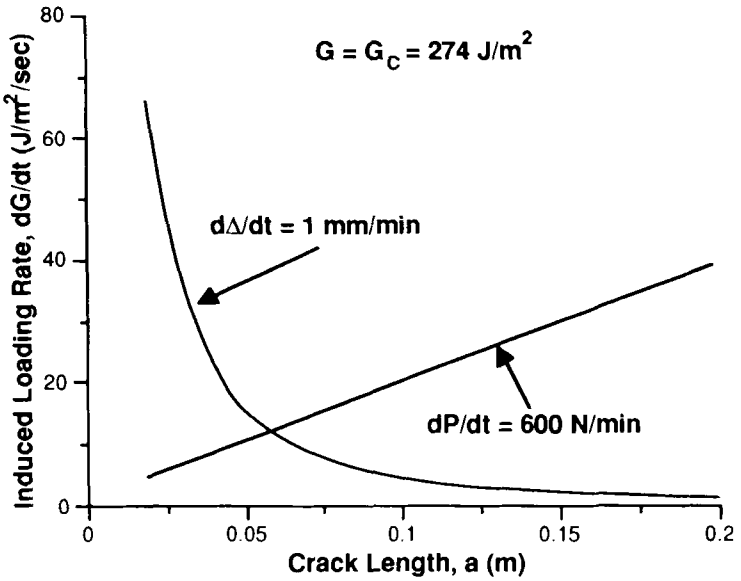

FIGURE 6 Induced (crack tip) loading rate just prior to failure at G_c as a function of crack length (Adhesive D).

where c_1 and n are considered to be material system constants under the given testing conditions. An example of applying this technique to interfacial debonding of one of the present adhesive systems is shown in Figure 7. These results were obtained during the time-dependent debonding (*i.e.* point 3 to point 4 in Fig. 3) at constant displacement for several loading cycles on the same specimen. Although a linear fit of the data can be made using this procedure, different loading cycles produced shifted data, with longer crack lengths resulting in data shifted to the left. This systematic shift of the data, typical for most specimens tested in this research program, suggests that Eq. 11 may not be appropriate for interfacial failures in our particular adhesive system. Since the cross-head was fixed during each of these debonding events, the only apparent explanations would be that Eq. 11 is not applicable or that some type of a process zone effect may have been occurring.[36] Since the crack lengths were quite large, we have had difficulty justifying that the process zone was continuing to change. We did find that the plastic zone sizes produced were probably smaller than the bond thickness for most of the model adhesives.

Although there are good theoretical reasons for utilizing da/dt to model some time dependent fracture events, the particular form expressed in Eq. 11 appears to be empirical. Seemingly, one could propose other models, also empirical, to describe the time dependence. A complimentary approach focused on experimentally determining crack growth rate in terms of the natural unloading rate, $(\dot{G})_\Delta$. Figure 8 was obtained when the same data from Figure 7 was plotted in terms of $(\dot{G})_\Delta$ *versus* the strain energy release rate. Note that the curves from the various loading cycles are much tighter in Figure 8 than in Figure 7. Similar results were obtained for all of the model adhesive

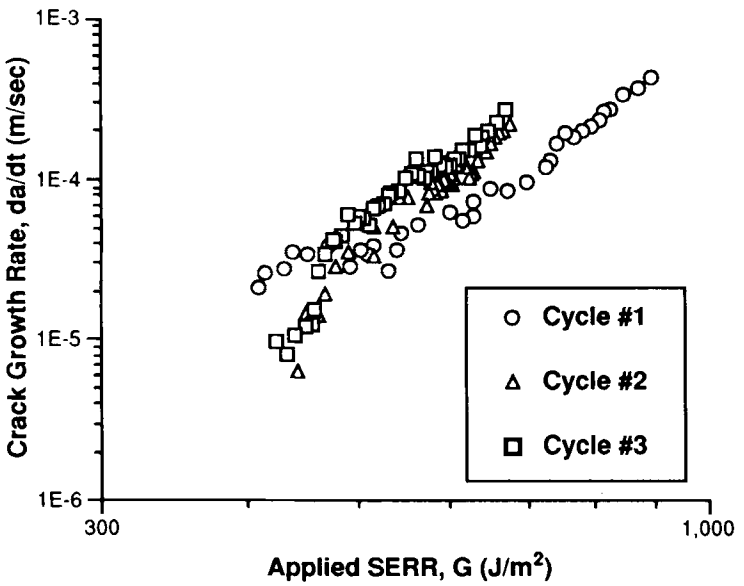

FIGURE 7 Crack growth rate as a function of applied strain energy release rate (SERR) under fixed displacement conditions (Adhesive E).

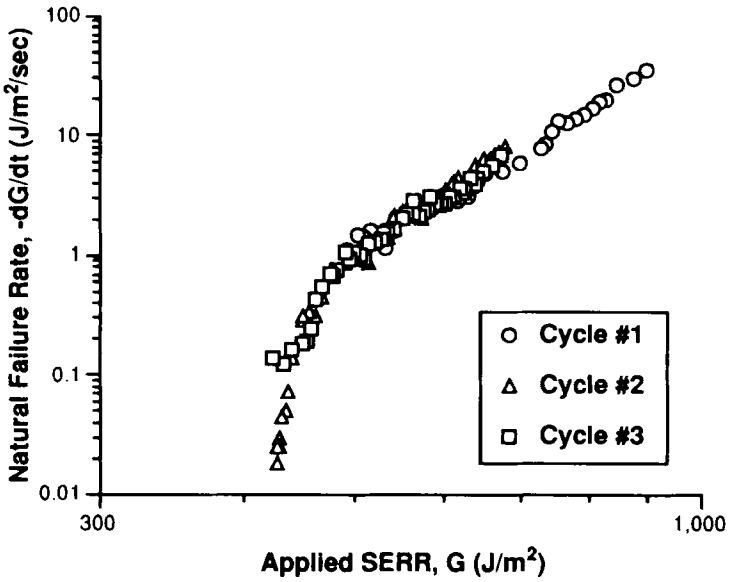

FIGURE 8 Natural unloading rate due to crack growth as a function of applied strain energy release rate (SERR) (Adhesive E). Data correspond to those of Figure 7.

systems studied. Based on the improved consistency in the data when plotted according to this criterion, we propose an alternate model:

$$(\dot{G})_\Delta = -A \cdot G^z \tag{12}$$

where A and z are considered to be system constants (at the given test conditions) which characterize the natural unloading rate due to crack growth.[§] The negative sign in Eq. 12 is required since the DCB specimen is unloaded as a result of crack growth. Throughout the remainder of the paper, this term will be referred to as the natural failure process, as it represents the "natural" debonding response under fixed displacement conditions.

Since $(\dot{G})_\Delta$ has been modeled explicitly, Eq. 8 can now be written as:

$$\dot{G} = \frac{3\dot{\Delta}}{(a+x)^2}\sqrt{\frac{G(EI)_{\text{eff}}}{B}} - AG^z. \tag{13}$$

Thus, the net loading rate, $\dot{G}$, is given as a function of the opening displacement rate, $\dot{\Delta}$, specimen geometry (crack length, etc.), the applied strain energy release rate, G, and the new system constants A and z used to characterize the failure rate. The traditional crack growth rate may be expressed as:

$$\frac{da}{dt} = A\frac{(a+x)}{4}G^{z-1} \tag{14}$$

[§] Equation 12 models only the response between the threshold and critical values of the strain energy release rate, although a more general modeling approach, such as the one used by Kinloch and Osiyemi[37] for fatigue data could be used.

and is thus a linear function of strain energy release rate, G, as well as crack length, a, as has been observed in Figure 7. It is important to note that Eq. 11 and 12 are not consistent with one another if the c_1 and A are assumed to be independent of the crack length. Thus, they are not different forms of the same expression, but represent fundamentally different assumed forms of time dependence. Because the criterion presented in Eq. 12 is more consistent with the data, it will be used in the remaining modeling.

A Time Marching Scheme to Model the Interfacial Failure Process

The resulting model from the previous section can be used along with a time marching technique to simulate numerically how all the rate-dependent components interact with each other and influence the complete mechanical response of a DCB specimen as it fails. If the specimen geometry, global testing rate, and loading level are known at some value of time, this rate-dependent model can calculate the time rate of change of these components at that instant, and predict the values after some increment in time.

It is first necessary to define initial conditions at time t_0, such as the initial crack length, a_0, and either the initial strain energy release rate level, G_0, or opening displacement, Δ_0 (since the other can be calculated from Eq. 1b). The following time marching equations are used to model t, Δ, and a:

$$t_{i+1} = t_i + \mathrm{d}t \tag{15}$$

$$\Delta_{i+1} = \Delta_i + \left(\frac{\mathrm{d}\Delta}{\mathrm{d}t}\right)_i \mathrm{d}t \tag{16}$$

$$a_{i+1} = a_i + \left(\frac{\mathrm{d}a}{\mathrm{d}t}\right)_i \mathrm{d}t \tag{17}$$

Note that $\mathrm{d}\Delta/\mathrm{d}t$ is the controlled opening displacement rate which is usually either constant during loading, or zero when the displacement is held constant. For simplicity it will be assumed that $G_a \approx G_c$ and that crack growth, $\mathrm{d}a/\mathrm{d}t$, only occurs when $G \geq G_c$, and thus:

$$\left(\frac{\mathrm{d}a}{\mathrm{d}t}\right)_i = \begin{cases} 0 & (G < G_c) \\ \dfrac{A(a_i + x)(G_i)^{z-1}}{4} & (G \geq G_c) \end{cases} \tag{18}$$

Equations 16 and 17 can be used along with Eq. 1b to calculate the G values. Similarly the load P can be computed by:

$$P = \frac{3\Delta(EI)_{\mathrm{eff}}}{2(a + x)^3} \tag{19}$$

RESULTS AND DISCUSSIONS

Rate-Independent Versus (Real) Rate-Dependent Failures

It is interesting and useful to compare actual failure processes with the rate-independent failure processes which are sometimes assumed. A rate-independent analysis assumes the specimen fails at some critical loading level, G_c, *and* the failure proceeds such that the loading level remains constant at G_c. Mathematically, the rate-independent failure process requires the following condition during sustained failure:

$$\left.\frac{dG}{dt}\right|_{G=G_c} = 0 \tag{20}$$

Figure 4 showed actual experimental data for Adhesive D along with two predicted load-deflection curves which assume the DCB specimen fails in a rate-independent manner. The rate-independent, iso-G curves assume the specimen failed at either the average maximum or arrest strain energy release rate loading levels obtained from experiments. By comparing the data in Figure 4, it is obvious that the DCB specimens tested in this research did not fail in such a rate-independent manner. It should be noted that this behavior was not due to the fact that we cycled the specimen through several load-hold-unload cycles. Figure 9 shows a similar trend for a specimen which was loaded continuously at a constant displacement rate.

Predicting Interfacial Load-Deflection Curves

Although the present rate-dependent failure model offers a qualitative explanation for all of the interfacial experimental observations previously listed, in the present paper

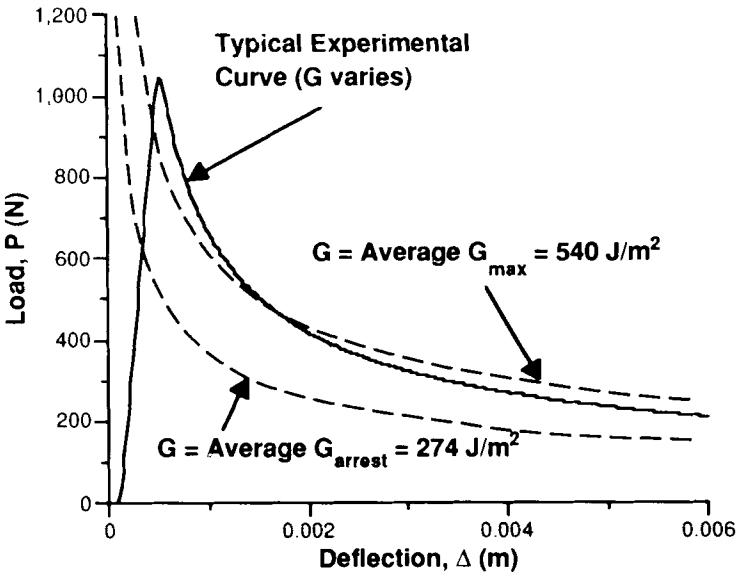

FIGURE 9 Rate-independent (iso-G) and real load-deflection curves obtained by maintaining a constant crosshead displacement rate.

we will concentrate on the more quantitative results to illustrate the utility of the model. For a more detailed examination of particular experimental observations, see Ref. 25. Table II contains the data necessary for applying the interfacial rate-dependent failure model to the Adhesive D sample used as an example earlier in this paper.

As a more critical test of the present model, we have used the natural failure rate parameters z and A obtained from the first hold cycle of this DCB sample to predict the failure of the specimen during the remainder of the test. A better correlation between the experimental and predicted data can generally be obtained if the average z and A values are used to make the predictions. However, a reasonable fit is still observed when the values from a single hold cycle are used. Note that no curve fitting is used to produce any of these predictions since the variables z and A are determined during the fixed crosshead portion of the first loading cycle of the DCB test (at which time $\dot{\Delta}$ is zero). Figure 10 allows comparison of the experimental results and predicted load-deflection curves when the present analysis technique is used**.

Figure 11 illustrate the effects on the predicted load-deflection curves when the crosshead displacement rate is altered. Again, only the z and A values obtained from the first hold cycle are used to make the predictions. As would be expected, the predictions for the testing rate equal to that of the actual experimental testing rate are in best agreement. The 0.001 mm/min results are jagged because the global testing rate is so slow that the predicted values simply oscillate about G_c.

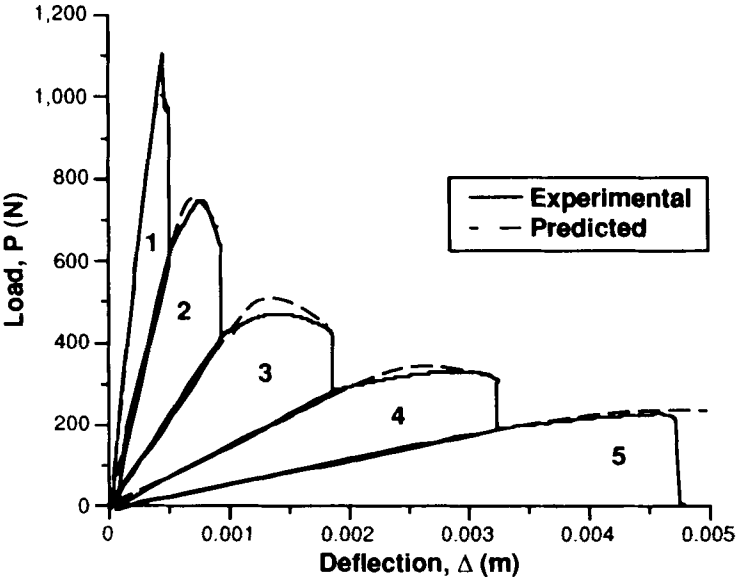

FIGURE 10 Experimental and predicted load-deflection curves for Adhesive D.

** The disagreement between experimental and predicted curves for loading cycle #3 is due to the fact that the crosshead was momentarily held shortly after exceeding G_c. Unfortunately, this fact is hidden by the predicted curve.

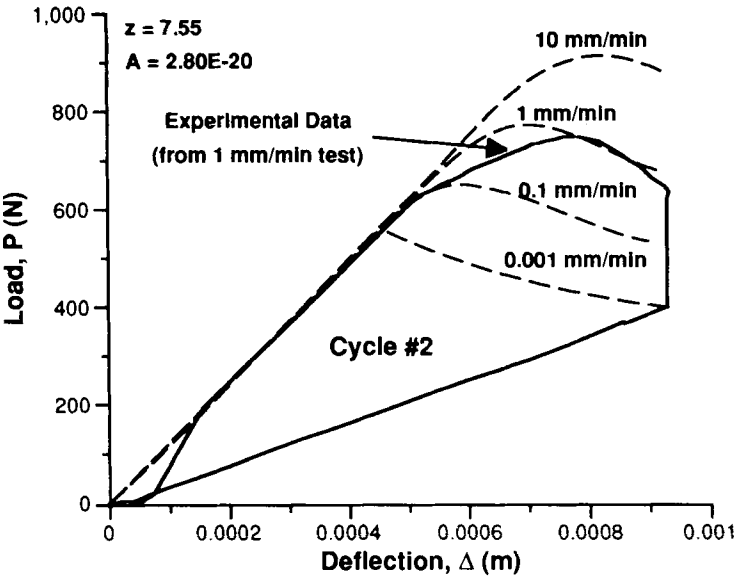

FIGURE 11 Effect of loading rate on the predicted load-deflection curves for loading cycle #2.

The fact that this curve is near G_c is illustrated by the curve approaching the point at which crack growth arrested for this loading cycle. Also, the predicted curve does not gradually reach a maximum after deviating from linearity at the point of crack initiation. Such quasi-rate-independent failures could perhaps be produced from a very slow test.

Figure 12 shows what effects different z values (natural failure rates) might have on the results of a DCB test which is conducted with a constant crosshead displacement rate of 1 mm/min. Again, the jagged curve is oscillating about the critical strain energy release rate. However, this time it is due to a higher natural failure rate instead of a lower testing speed. Note that relatively small changes in the z values are sufficient to produce significant changes in the predicted load-deflection curves. Finally, the predicted curve with the closest agreement to the experimental data is again produced using the z value obtained from the first hold cycle of this specimen.

Interfacial G_{max} Predictions

As previously mentioned, the experimental G_{max} values consistently decreased as a test progressed using a constant crosshead displacement rate to conduct the test. In this section we will use the present rate-dependent failure model to predict the maximum attainable strain energy release rate for different loading cycles of a DCB test and compare the results with experimental values. The approach is relatively straightforward in that we will use the fact that G is an extreme (maximum) when $\dot{G} = 0$. Therefore, by setting Eq. 10 equal to zero and solving for G we get:

$$G_{max} = \frac{9(EI)_{eff}}{16B(a+x)^2}\left(\frac{\dot{\Delta}}{\dot{a}}\right)^2 \tag{21}$$

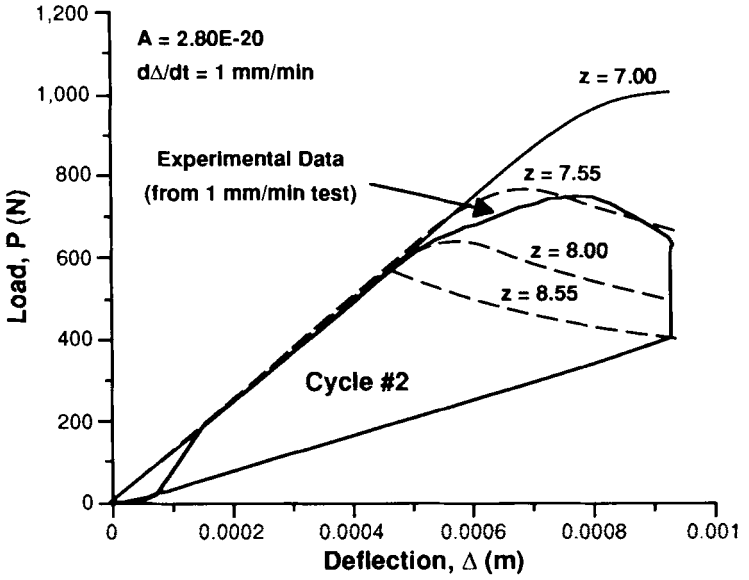

FIGURE 12 Effect of z values on the predicted load-deflection curves for loading cycle #2.

where G now becomes G_{max}. Eq. 21 shows that the maximum attainable loading level is a function of specimen geometry (including crack length), the global testing rate, and the crack growth rate. Substituting Eq. 15 into Eq. 21 we get an equation for G_{max} in terms of the natural failure rate parameters z and A:

$$G_{max} = \left(\frac{3\dot{\Delta}}{A(a+x)^2} \sqrt{\frac{(EI)_{eff}}{B}} \right)^{2/(2z-1)} \tag{22}$$

Equation 22 could have also been obtained by setting Eq. 14 equal to zero and solving for G_{max}. However, Eq. 21 illustrates the influence of the crack growth rate, with which we are most familiar when discussing failure rates.

Figure 13 shows the results of applying Eq. 22 to the present sample being used as an example where the experimental values were obtained from a 1 mm/min test. As seen in Figure 13, there is a good correlation between the predictions and experimental data for the same testing speed. Again, only rate-dependent debonding data under fixed displacement conditions during the first loading cycle were used to make the predictions for the subsequent cycles. Similar agreement was obtained for the other adhesive systems as well.

Including Cohesive Fractures in the Failure Model

The only observations which we have yet to explain with the rate-dependent model are the observations that deal with cohesive fractures and the ability to switch back and forth between interfacial and cohesive fracture modes by simply altering the testing

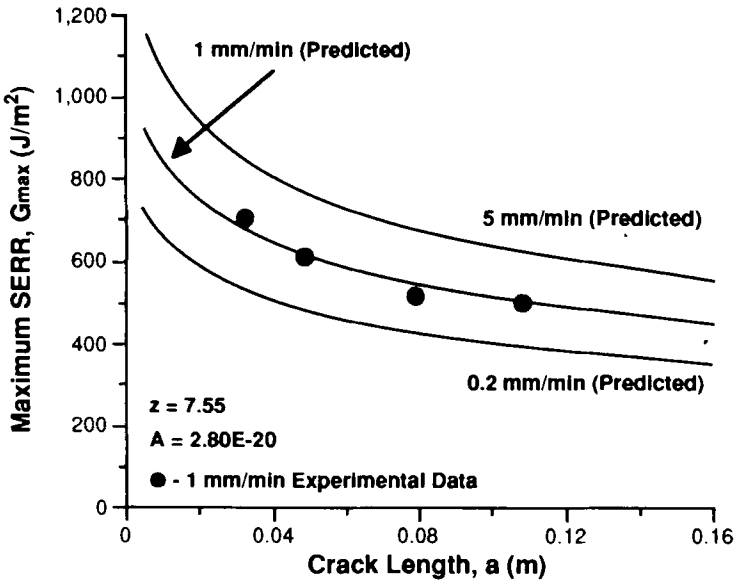

FIGURE 13 Predicted and experimental maximum strain energy release rate (SERR) values as a function of crack length and crosshead displacement rate (Adhesive D).

rate. In this section we will offer an explanation why these peculiar failure characteristics exist in the present adhesive systems as well as why the observed cohesive fracture trends are as they are. Specifically, we will: (1) explore aspects of the interfacial model that illustrate why the cohesive fractures are possible and why it is possible to switch back and forth between interfacial and cohesive fractures, (2) suggest a reason for the trend observed in the cohesive fracture energies, (3) model the cohesive fracture trends and incorporate them into the present interfacial rate-dependent fracture model, and (4) present a failure envelope which can be used to predict whether a fracture will be interfacial or cohesive, depending on the adhesive system's failure characteristics (interfacial and cohesive), specimen geometry, and the global testing rate.

Recent research suggests that an adhesively bonded joint may not necessarily fail in what appears to be its weakest region.[38-40] Instead, under certain circumstances the crack is expected to select a trajectory in the joint such that its local mode II loading, K_{II}, is zero, when possible, Wang and Suo[39] found that when the crack tip was loaded primarily in mode I, with only a small component of mode II loading, fracture tended to occur within the adhesive layer, even though the interfacial toughness of the system may have been lower than that of the bulk adhesive. Subsequently, Fleck *et al.*[40] investigated the influence of various mixed-mode loadings and residual stresses on the possible crack path selections within an adhesive joint. In these works it was shown that the same adhesive system can fail either interfacially or cohesively, depending on the local loading conditions. Furthermore, the work of Wang and Suo illustrated that in some instances it was possible to attain interfacial G values which were higher than some of the cohesive failure values.

The present work does not dispute these findings, but merely suggests how viscoelastic behavior may complicate the elastic analyses mentioned above. In fact, for our model systems, it is suspected that rate dependent behavior of the bulk polymer is very different than for the interphase region. We do attempt to explore and isolate aspects of the rate-dependent interfacial failure characteristics observed in the present adhesive systems to show that the local loading rate can also contribute to the initiation (or suppression) of cohesive fractures. Specifically, we will investigate why variations in the induced loading rate can cause failures to switch back and forth between interfacial and cohesive failure modes. Where the crack is expected to go within the adhesive layer once cohesive fracture is initiated will not be addressed here. However, once cohesive failures were initiated in the present adhesive systems, some of the peculiar crack path selections which are predicted by Fleck *et al.*[40] were, in fact, observed.

Any complete analysis for crack path selection should account for both the stress field (including singularities), and the spatially-dependent strengths or toughnesses. To avoid the complexities addressed in Refs. 38–40, however, we will make a simplification, assuming that the DCB specimens fail at their weakest link; either at the adhesive/adherend interface (or interphase region) or cohesively within the adhesive layer. However, depending on the combination of the applied strain energy release rate and the induced loading rate, the weakest link may change as the specimen fails. In addition to the interfacial fracture energies already defined, independent cohesive fracture energies are also assumed to exist for the present adhesive systems. The critical strain energy release rate associated with the onset of cohesive fracture will be denoted by G_c^c and the loading level associated with cohesive crack arrest will be denoted by G_a^c, where the "c" superscript refers to cohesive fracture values. Although the G_c^c values also displayed some rate dependence which will be discussed later, for the present discussion we will simply assume that G_c^c exists and that it is higher than the interfacial fracture value of G_c. This convention was chosen because the G_c^c cohesive fracture values for the present adhesive systems were usually much higher than the interfacial fracture values of G_c[††]. It is evident that if G_c^c is substantially greater than G_c and rate-independent failure occurs, then it is impossible for the strain energy release rate to reach G_c^c. However, after closely examining the behavior characteristics of the rate-dependent failure model presented in this paper, it becomes apparent that such rate-dependent failures makes it *possible* for the crack tip to reach loading levels substantially higher than G_c. Specifically, since Eq. 22 predicts higher interfacial strain energy release rate can be achieved if (1) faster crosshead displacement rates are used, (2) shorter crack lengths are present, and (3) when an adhesive system has a slower natural interfacial failure rate (*i.e.* lower values of z and A), Eq. 22 also predicts that conditions sufficient to cause cohesive fractures might eventually be satisfied as interfacial failures proceed. Therefore, it would be possible to reach G_c^c and generate cohesive failures *after* interfacial failures are initiated. Whether or not this transition in failure mode would actually take place would depend on all of a system's fracture characteristics, both interfacial and cohesive, as well as the strain energy release rate used to fail the joint.

[††] On average, the interfacial fracture values were only about 17.5% as tough as the bulk adhesives as determined from Single Edge Notched Bend (SENB) tests. As expected, the G_c^c values obtained from the DCB tests were similar to the critical fracture energies obtained from the SENB tests.

These observations suggested that it might be possible to take adhesive systems that had always failed interfacially in previous tests and cause them to fail cohesively by sufficiently increasing the crosshead displacement rate. Similarly, it might also be possible to take systems which had always failed cohesively in previous tests and produce interfacial failures by testing them very slowly. Therefore, we went back and retested the adhesive systems used in this research and were able to produce both interfacial and cohesive fractures in all of the systems by simply altering the testing rates accordingly.

Explaining the Trend Observed in the Cohesive Fractures

As pointed out earlier, there was a trend for cohesive failures to occur at higher strain energy release rates at longer crack lengths under constant displacement rate loading, presumably because of the effect of crack length on the induced loading rate. This is quantitatively depicted in Figure 14, where DCB cohesive failure data is plotted along with the $G_c (= G_a)$ and G_{max} interfacial fracture energies obtained from slower DCB tests, and the bulk adhesive fracture energies obtained from SENB tests on this same adhesive system. One of the most interesting observations was that slower loading rates tended to reduce the measured strain energy release rate for the interfacial failures, but increase the toughness of cohesive failures. For a given polymer, such trend reversals are often seen when one passes through a transition. Thus, above the T_g the rubbery polymer may become stronger with increasing loading rate, while the glassy polymer (below T_g) may become weaker (more brittle) with increasing loading rate. (Such observations have been reported for joint tests in Refs. 4 and 6–10 and for bulk

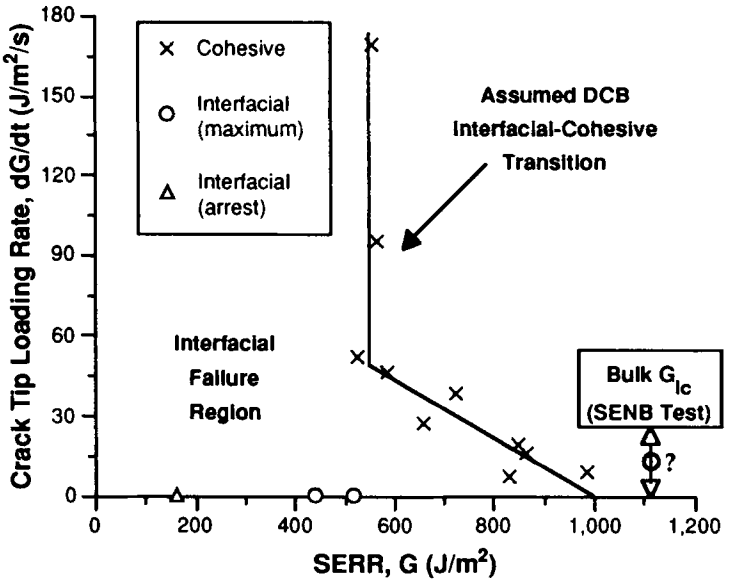

FIGURE 14 Fracture energies as a function of induced loading rate (Adhesive C).

adhesives in Refs. 6 and 7.) Since our specimens were all tested at a single temperature, however, this apparent trend reversal may suggest that the viscoelastic nature of the bulk adhesive and interphase region are quite different. Perhaps migration of certain species to the steel interface[23] may have altered the stoichiometry enough to result in fundamentally different materials in these two regions.

Modeling and Predicting Cohesive Fractures

Just as it is not possible to control the natural interfacial failure rates, it is not possible to control when the rate-dependent cohesive fractures occur. Therefore, the rate-dependent cohesive fractures must also be determined from experimental results. Due to the relative brittleness of the present bulk adhesive systems, the time between cohesive crack initiation and crack arrest was very short (less than 0.1 sec). Because of this, no attempt was made to model the failure rate of the cohesive failures in great detail. Instead, it was simply assumed that the jump from G_c^c to G_a^c occurs instantaneously. Note that if a particular system does not obey the present failure characteristics, one could easily model the rate at which cohesive failure occurs and incorporate it into the present model.

As Figure 14 shows, the cohesive fracture energies obtained from DCB tests on Adhesive C can be modeled reasonably well as a bi-linear function of the strain energy release rate. By viewing the lines shown in Figure 14 as the transition between interfacial and cohesive fracture modes for DCB specimens containing Adhesive C, the failure mode can be modeled as a two-parameter problem where the type of failure, either interfacial or cohesive, depends on the *combination* of the strain energy release rate as well as the rate of change in the loading level (*i.e.* the failure mode $= f(G, \dot{G})$. For example, if the pair $(G, \dot{G})$ lies to the left of the lines in Figure 14, then interfacial failure is assumed to occur. However, if the combination ever meets the transition lines, cohesive failures are expected. Due to the nature of the present cohesive fractures (almost instantaneous drops in load from G_c^c to G_a^c), it would not be possible to obtain cohesive fracture values very far to the right of the transition lines. Interestingly, it appears that the rate-dependent interfacial failure process allows for interfacial failures to occur at any combination of G and $\dot{G}$ as long as $G \geq G_c$ and the pair lies to the left of the interfacial-cohesive transition lines of Figure 14.

Now that the interfacial to cohesive fracture transition can be modeled reasonably well, it can be incorporated into the interfacial failure model by adding the following stipulation to Eq. 20:

$$\left(\frac{da}{dt}\right)_i = \frac{\sqrt[4]{\dfrac{9\Delta_i^2 (EI)_{\text{eff}}}{4BG_a^c}} - x - a_i}{dt} \tag{23}$$

Equation 23 is only valid when the pair $(G, \dot{G})_i$ lies on (or above) the interfacial-cohesive transition and it simply defines da/dt such that the modeled crack jumps to a crack length corresponding to a strain energy release rate of G_a^c for the current crosshead displacement. Figures 15 and 16 illustrate predictions for a system which contains Adhesive C when these additions are made to the rate-dependent failure model. The

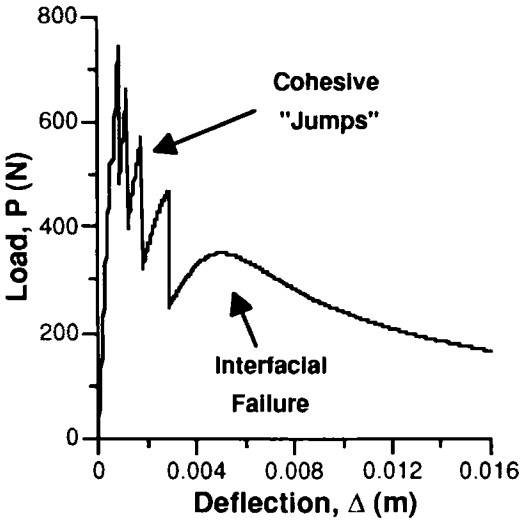

FIGURE 15 Predicted load-deflection curve ($d\Delta/dt$ = 1 mm/min, z = 3.639, and A = 6.602E-11).

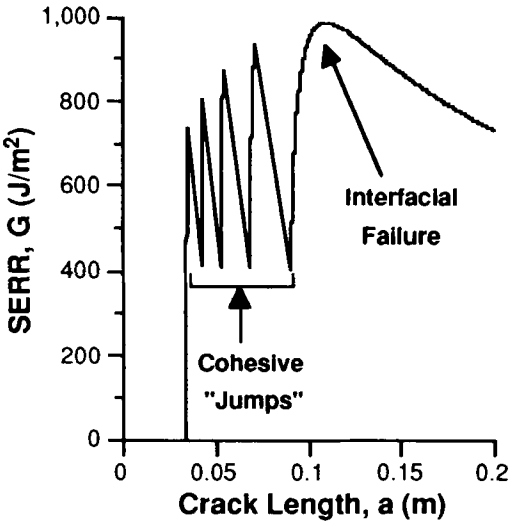

FIGURE 16 Predicted strain energy release rate (SERR) *vs.* crack length curve ($d\Delta/dt$ = 1 mm/min, z = 3.639, and A = 6.602E-11).

interfacial-cohesive transition was modeled as the lines shown in Figure 14 while the interfacial failure characteristics (G_c, z, A, etc.) were obtained from slower DCB tests which produced interfacial failures in these samples. Since the crosshead displacement rate used to produce Figures 15 and 16 remained constant at 1 mm/min, any induced

loading rate differences and, consequently, failure mode differences, are obviously a result of different crack lengths. Many times in cohesive failures, cracks propagate in a fast stick-slip manner. This might explain the cohesive jumps seen in Figures 15 and 16. Note that, although they are similar in appearance, the vertical load drops in Figure 15 occur almost instantaneously, while they occur over longer periods of time when interfacial failures occur as in Figure 3. Figure 16 shows the interesting prediction that, under certain test conditions, it is possible to obtain higher interfacial strain energy release rate than for some cohesive failures in the same sample. As Figure 14 shows, this was achievable in the present study.

An Interfacial-Cohesive Failure Envelope

It is possible to proceed one step further and state that, if the interfacial fracture characteristics are known along with the shape and position of the interfacial-cohesive transition, then it is possible to predict whether interfacial or cohesive fracture will occur for a given testing speed and test specimen geometry. The prediction method utilizes essentially the same analysis procedure as was used to produce Figures 15 and 16. In order to determine whether or not cohesive failure is likely to occur, we simply need to model the interfacial failure of a system and produce the $\dot{G}$ *versus* G curves for given specimen geometries and testing speeds and then determine their relationship to the interfacial-cohesive transition curve. If an interfacial loading rate curve crosses the interfacial-cohesive transition line(s), then cohesive fracture is expected to occur at the point of intersection. Figure 17 shows the predictions for different initial crack lengths

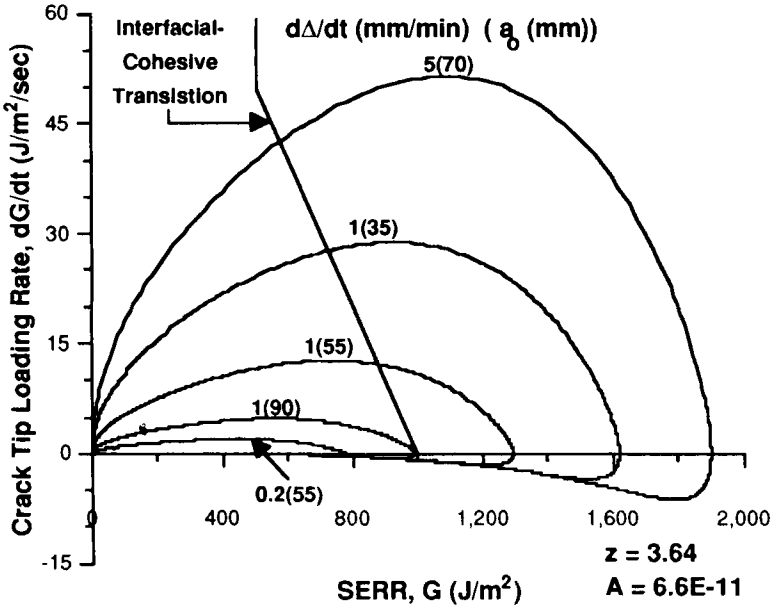

FIGURE 17 Net loading rate as a function of strain energy release rate for different initial debond lengths and testing speeds (Adhesive C).

and testing speeds when testing the adhesive system used to produce Figures 15 and 16. The smallest loading loop would be expected to produce only interfacial failures. The second loading loop is on the verge of going cohesive, whereas the three largest loading loops could be expected to produce cohesive failures once the envelope is reached.

Although the program used to create Figures 15 and 16 gives the data necessary to produce Figure 17 with both the interfacial and cohesive failures present, such a Figure is not presented because the assumed instantaneous drop in load from G_c^c to G_a^c creates huge negative dG/dt values when the cohesive fractures occur. This produces scale differences which make the positive portions of the graphs illegible. Therefore, only the interfacial failure characteristics are presented along with the interfacial-cohesive transition.

CONCLUSIONS

Time-dependent debonding has been reported for double cantilever beam specimens bonded with several model epoxy/steel adhesive systems. Cohesive fracture strengths of the DCB specimens were considerably higher than interfacial values, and corresponded quite well with bulk polymer toughness. Interfacial debonding predominates at lower loading rates, and cohesive failures were routinely induced by increasing the loading rates. The time dependence of the interfacial debonding resulted n increased energy consumption at higher debond rates, whereas the rate effect of the cohesive failures were just the reverse. This reversal of time dependence trends for interfacial and cohesive failures may suggest quite different material chemistry/properties in the interphase region.

The classical crack propagation model based on the debond rate being proportional to the strain energy release rate raised to some power was found to produce inconsistent results for the interfacial failures observed herein. An alternate approach was proposed in which the rate of decrease in the applied strain energy release rate (under fixed grip conditions) is proportional to some power of the strain energy release rate. Although the applicability of this model to other adhesive systems is not known, it did produce more consistent results for the adhesive systems studied herein.

The observed rate-dependent failure events have been modeled in terms of the time rate of change of the strain energy release rate, the combined effect of the mechanically-induced loading rate with the natural debonding failure rate. The natural failure rate is believed to be a fundamental indication of a system's fracture behavior and, as might be expected, the parameters used to characterize it (*i.e.* z and A) were found to be dependent on many system variables such as adhesive and surface chemistries, testing conditions, and environmental conditioning. After quantifying the natural failure rate, the model was used to predict the mechanical response of DCB specimens subjected to various crosshead displacement rates. In general, these interfacial failure predictions were found to be in good agreement with experimental observations.

The transition between interfacial and cohesive fractures was modeled in terms of the time rate of change of the applied strain energy release rate. This information was then combined with the interfacial failure process to predict whether failures would be interfacial or cohesive in nature, depending on the DCB specimen geometry and global

testing speed. A proposed failure envelope may be useful in determining whether failure will be interfacial or cohesive for a given adhesive system.

In conclusion, the present work illustrates that the time rate of change of the strain energy release rate can have significant implications to adhesive testing techniques when rate-dependent interfacial failures exist, because not only can the maximum fracture values be altered, but the mode of failure can also be changed by simply changing the global testing rate. A better understanding of these rate-dependent interfacial failures could play an important role in developing long-term durability prediction models for bonds. Although the time scales used herein for the laboratory testing were quite short, extensions to longer times for durability predictions may be possible with further studies.

Acknowledgements

The authors would like to thank The Dow Chemical Company for contributing financial support and experimental materials to this project. Additional financial support was received from The Adhesive and Sealant Council Education Foundation. The Center for Adhesive and Sealant Science, and the Virginia Institute for Material Systems. Finally, we also recognize the benefit obtained through the interdisciplinary research environment established in part through the National Science Foundation Science and Technology Center: High Performance Polymeric Adhesives and Composites, Contract DMR 9120004. In addition, laboratory assistance from Kiersten Urban is gratefully acknowledged.

References

1. B. Dattaguru, R. A. Everett, Jr., J. D. Whitcomb and W. S. Johnson, *J. Eng. Mater. and Tech.* **59,** 106 (1984).
2. C. K. Riew, E. H. Rowe and A. R. Siebert, *Toughness and Brittleness of Plastics, ACS Adv. Chem. Ser.* **154** (American Chemical Society, Washington, D.C., 1976).
3. C. B. Bucknall and T. Yoshii, *British Polym. J.* **10,** 53 (1978).
4. A. J. Kinloch, S. J. Shaw, D. A. Tod and D. L. Hunston, *Polymer* **24,** 1341 (1983).
5. A. J. Kinloch, S. J. Shaw and D. L. Hunston, *Polymer* **24,** 1355 (1983).
6. Y. Huang and A. J. Kinloch, *J. Adhesion* **41,** 5 (1993).
7. A. A. Khalil and M. R. Bayoumi, *Eng. Fract. Mech.* **39,** 1037 (1991).
8. A. J. Kinloch and S. J. Shaw, *J. Adhesion* **12,** 59 (1981).
9. V. T. Truong, *Polymer* **31,** 1669 (1990).
10. S. Mostovoy and E. J. Ripling, *J. Appl. Polym. Sci.* **10,** 1351 (1966).
11. J. L. Bitner, J. L. Rushford, W. S. Rose, D. L. Hunston and C. K. Riew, *J. Adhesion* **13,** 3 (1981).
12. P. A. Fay and A. Maddison, *Int. J. Adhesion and Adhesives* **10,** 179 (1990).
13. T. Horton, G. M. Spinks and N. A. Isles, *Polym. Int.* **28,** 9 (1992).
14. A. J. Kinloch, *J. Adhesion* **10,** 193 (1979).
15. S. Mostovoy and E. J. Ripling, *J. Appl. Polym. Sci.* **13,** 1083 (1969).
16. J. F. Watts, J. E. Castle and T. J. Hall, *J. Mater. Sci. Lett.*, **7,** 176 (1988).
17. S. G. Hong and F. J. Boerio, *J. Adhesion* **32,** 67 (1990).
18. R. A. Schapery *Int. J. Fracture* **25,** 195 (1984).
19. R. A. Schapery, *Int. J. Fracture* **11,** 141; 369–549 (1975).
20. W. G. Knauss, *Deformation and Fracture of High Polymers*, H. H. Kausch, *et al.*, Eds. (Plenum, New York, 1974).
21. W. G. Knauss and G. U. Losi, *J. Appl. Mechanics* **60,** 793 (1993).
22. A. N. Gent and R. P. Petrich, *Proc. Royal Soc.* **A. 310,** 433 (1969).
23. D. Maugis, *J. Materials Science* **20,** 3041 (1985).
24. M. A. Vrana, Ph.D. Dissertation, Virginia Polytechnic Institute and State University, 1995.
25. M. D. Rakestraw, Masters Thesis, Virginia Polytechnic Institute and State University, (in progress).
26. M. D. Rakestraw M. A. Vrana, T. Chang, D. A. Dillard, T. C. Ward and J. G. Dillard, *Evaluation of Adhesive Performance Using Static, Fatigue, and Environmental Fracture Testing*, 1993 ASC Graduate

Fellowship Report-CASS/MESc/94-2, The Center for Adhesive and Sealant Science, Blacksburg, VA, May 1994.
27. M. D. Rakestraw M. A. Vrana, D. A. Dillard, J. G. Dillard and T. C. Ward, *Durability and Damage Tolerance, AD*-Vol. **43,** ASME WAM, 65 (1994).
28. M. D. Rakestraw, M. W. Taylor, T. Chang and D. A. Dillard, *Journal of Engineering Materials and Technology*, to be submitted.
29. B. Blackman, J. P. Dear, A. J. Kinloch and S. Osiyemi, *J. Mater. Sci. Lett.* **10,** 253 (1991).
30. *ASTM*, D3433-93, Annual Book of ASTM Standards, Volume **15.06** Adhesives, 218 (1994).
31. J. G. Williams and G. P. Marshall, *Proc. R. Soc. Lond. A.* **342,** 55 (1975).
32. S. F. Popelar, C. H. Popelar and V. H. Kenner, *Advances in Electronic Packaging ASME*, 619 (1992).
33. K. M. Conley, J. E. Ritter and T. J. Lardner, *J. Mater. Res.* **7,** 2621 (1992).
34. S. Mostovoy and E. J. Ripling, *Fracturing Characteristics of Adhesive Joints, Final Report*, Materials Research Laboratory, Inc., Glenwood, IL, July 1972.
35. G. P. Anderson, S. J. Bennett, K. L. DeVries, *Analysis and Testing of Adhesive Bonds* (Academic Press, New York, 1977).
36. S. Ostlund and F. Nilsson, *Fatigue and Fracture of Engineering Materials and Structures* **16** (6), 663 (1993).
37. A. J. Kinloch and S. O. Osiyemi, *J. Adhesion* **43,** 79 (1993).
38. H. C. Cao and A. G. Evans, *Mech. Mater.* **7,** 295 (1989).
39. J. S. Wang and Z. Suo, *Acta Metall.* **38,** 39 (1990).
40. N. A. Fleck J. W. Hutchinson and Z. Suo, *Int. J. Solids Structures* **27,** 1683 (1991).